

## **INFLUENCE OF LIQUID MEDIUM ON LASER ABLATION OF TITANIUM**

Barbora BOČÁKOVÁ<sup>1</sup>, Martin NECPAL<sup>1</sup>, Martin SAHUL<sup>2</sup>

<sup>1</sup>SLOVAK UNIVERSITY OF TECHNOLOGY IN BRATISLAVA  
FACULTY OF MATERIALS SCIENCE AND TECHNOLOGY IN TRNAVA  
INSTITUTE OF PRODUCTION TECHNOLOGIES  
ULICA JÁNA BOTTU 2781/25, 917 24 TRNAVA, SLOVAK REPUBLIC  
barbora.bocakova@stuba.sk, martin.necpal@stuba.sk

<sup>2</sup>SLOVAK UNIVERSITY OF TECHNOLOGY IN BRATISLAVA  
FACULTY OF MATERIALS SCIENCE AND TECHNOLOGY IN TRNAVA  
INSTITUTE OF MATERIALS SCIENCE  
ULICA JÁNA BOTTU 2781/25, 917 24 TRNAVA, SLOVAK REPUBLIC  
martin.sahul@stuba.sk

*Received 27 April 2022, Accepted 20 June 2022, Published 26 July 2022*

### **Abstract**

*Titanium grade 2 plates were modified by a pulsed nanosecond laser beam. The aim was to determine the surface properties after the machining process in two different liquid media. The samples were processed in distilled water and paraffin oil. It was found that a surface with half-surface roughness values with a number of cracks was formed in distilled water. The presence of water reduced the size of the heat-affected zone.*

### **Keywords**

*Laser micromachining, liquid environment, titanium*

### **INTRODUCTION**

Laser beam machining (LBM) is used to modify surfaces using the thermal removal mechanism of the surface layer. The thermal effect depends on thermal and optical properties of the workpiece and laser beam, workpiece and laser processing input parameters [1]. When a high-energy and high-intensity laser beam interacts with the workpiece, there is an optical breakdown at the solid surface and plasma, and a shock wave is formed. As a result of the shock wave, part of the molten material is ejected from the machined area. Then it solidifies in the form of drops. A smaller part of the material evaporates from the laser focal point, whereas the resulting upward vapours act on the molten material, generating the bubbles, which lead to further displacements of the melted micro- volumes [2]. Some major drawbacks of the nanosecond and microsecond pulsed lasers during materials processing are the thermal

damage of the machined surface and deep heat-affected zone. These disadvantages of laser beam machining in the air can be reduced to some extent by changing the working environment, e. g. vacuum, gasses, liquids [3, 4].

In contrast to laser ablation in air, the presence of a liquid layer above machined surface causes easier cooling because of its greater thermal conductivity than air. In addition, higher ablation efficiency can be achieved, which is attributed to the enhancement of energy-coupling efficiency, liquid-induced confinement on plasma, bubble motion, and formation of liquid shock waves. In the results, the morphology of the machined surface can be smoother, since debris is removed by thermal convection currents and bubble motion. The resulting material removal rate and morphology are related to liquid media properties, e. g. density, thermal conductivity, absorption coefficient at the incident laser wavelength, and liquid layer thickness.

Laser ablation in liquid (LAL) is applicable in engineering, medical and military industry [5]. Furthermore, laser ablation in liquid medium has been proven to be a very promising method for extracting nanoparticles and fabricating hydrides, carbides, and oxides grown by chemical reactions during machining [3, 4, 6]. Especially significant is the production of titanium nanoparticles, titanium oxides (piezoelectric crystals, fuel cells, sensors) [7] and titanium carbide (cut tool coatings) [8].

The researchers designed a wide range of experiments with different liquid media, e.g. alcohol, salty solutions, ethanol [9], etc. [1]. Semaltianos et al. [10] synthesized TiO nanoparticles by ps laser ablation in deionized water. The nanoparticles were formed in colloidal solutions with a median diameter of 10 nm. Serkov et al. [11] produced nanostructures using a picosecond laser, while the Ti target was in an external DC electric field and immersed in water. Albu et al. [12] observed different LIPSS on metallic surfaces immersed in water, ethanol, and chloroform during LAL. LIPSS were smaller and deeper than those produced by LBM in air. Chatuverdi et al. [13] formed polycrystalline in nature and spherical TiO<sub>2</sub> nanoparticles in Ti using pulsed laser ablation in deionized water and 0.001 M sodium dodecyl sulphate surfactant aqueous solution. Golightly et al. [14] observed titanium nanoparticles after LAL in water, ethanol, 2-propanol and n-hexane. Nanoparticles differ according to the liquid medium, e.g. NPs machined in water contained a higher amount of O<sub>2</sub>, NPs formed from n-hexane have higher carbon values.

The most widely used medium was deionized water due to its high heat capacity and thermal conductivity (with respect to air), low operating costs, and environmental friendliness [15]. Most of the authors focused on machining in a liquid medium to create nanoparticles and observe the chemical and phase composition down to the atomic level. However, less knowledge is available on microspheres and macrospheres. In the experiment described in this paper, the aim was to characterize the morphology of the titanium surface after machining in various liquid media.

## **MATERIALS AND METHODOLOGY OF EXPERIMENT**

### **Preparation of Experimental Samples**

As an experimental material, titanium grade 2 was chosen. Samples were prepared from metal sheet by cutting 15 x 6 x 1.5 mm sections. After cutting by a precision saw, the samples were ground by SiC paper P1200 grit. Then they were purified in alcohol for 15 minutes in ultrasonic cleaner. After laser modification, the samples were cleaned by ethanol and then alcohol in an ultrasonic cleaner. The samples were mounted for cross-sectional analysis into a conductive compound with edge retention. The cross sections were prepared metallographically by grinding, polishing and etching by a Kroll's etchant.

## Laser Modification of Surfaces

The sample surfaces were processed by a pulsed (Yb) nanosecond fibre laser by the Lasertec 80 Shape (DMG Mori) equipment. This five-axis machining centre for laser engraving achieves the maximum output power of 100 W and a maximum frequency of 100 kHz. The laser beam scanned the surfaces using a 3-layer cross-hatching strategy. The constant parameters of the laser sample modification process are given in Table 1.

<b>Table 1</b> Constant input parameters of laser modification	
<b>Wavelength</b>	1064 nm
<b>Pulse Duration</b>	120 ns
<b>Power</b>	72 W
<b>Frequency</b>	80 kHz
<b>Scanning speed</b>	2000 mm.s <sup>-1</sup>
<b>Focused beam diameter</b>	50 µm
<b>Lateral pulse overlap</b>	25 µm
<b>Transverse pulse overlap</b>	10 µm
<b>Energy density</b>	45.86 J.cm <sup>-2</sup>
<b>Modified area</b>	5 x 5 mm
<b>Machined layers</b>	3

During laser micromachining, the samples were placed in the fixture immersed in liquid medium (Fig. 1). As liquid media, distilled water and paraffin oil were applied. The monitored parameter was the thickness of the liquid layer above the sample surface; 1 and 3 mm high levels were monitored. The control sample was a surface modified with a laser beam in air. In this experiment, the samples were labelled as follows: C – control sample, modified without special atmosphere; W1 - modified sample 1 mm below water; W3 - modified sample 3 mm below water; O1 - sample modified 1 mm below paraffin oil; O3 - sample modified 3 mm below paraffin oil.



*Fig. 1 Prepared sample placed in the fixture*

## Samples Surface Analysis

The machined surfaces were analysed using the JEOL JSM 7600F high resolution scanning electron microscope (JEOL Ltd., Japan) in secondary electron imaging regime with following parameters:  $U = 15$  kV,  $I = 1$  nA and  $WD = 15$  mm using magnifications from 100 to 10,000 x. Samples were cleaned in acetone ultrasound bath prior the observation.

Wavelength-dispersive spectroscopy (WDS) was performed to determine the elemental composition of the processed surfaces. It was performed using the Inca Wave spectrometer (Oxford Instruments, High Wycombe, UK), which is a part of the above mentioned microscope. Prior to the quantitative analysis of the surfaces, the spectrometer was calibrated with C, SiO<sub>2</sub>, Ti and BN standards (Micro Analysis Consultants, St. Ives, UK). K $\alpha$  (C, O, N and Ti) lines were chosen for the quantification of X-ray data. The measured data were processed using INCA Wave software (Oxford Instruments, High Wycombe, UK).

Surface roughness parameters were measured using the ZEISS LSM 700 scanning laser confocal microscope (Carl Zeiss Microscopy GmbH, Germany). Surface 3D topography maps were processed using the Zeiss ConfoMap software (ConfoMap Premium 7.2, Digital Surf, Besançon, France). The dimensions of the measured area were  $0,937 \times 0,937$  mm<sup>2</sup>. The roughness parameters of the analysed area were the arithmetical mean of the height of surface (Sa), the mean square height of the surface (Sq), the maximum peak height (Sp), the maximum pit height (Sv) and the skewness of the scale-limited surface (Ssk), the kurtosis of the scale-limited surface (Sku) in according with the ISO 25 178 standard.

## ATTAINED RESULTS

### Scanning Electron Microscopy

The morphology of the surfaces was observed at the magnifications from 100 to 10,000. It was found that two representative surfaces were created on the machined surfaces. The first surface was characterized by globular formations and a roughly re-melted layer of the material. These surfaces are shown in Fig. 2 a) c), samples C and O1. Only the minimal amount of material removal can be observed on the surface of the O3 sample, characterized by irregular traces of the laser beam on the surface (Fig. 2 d)).

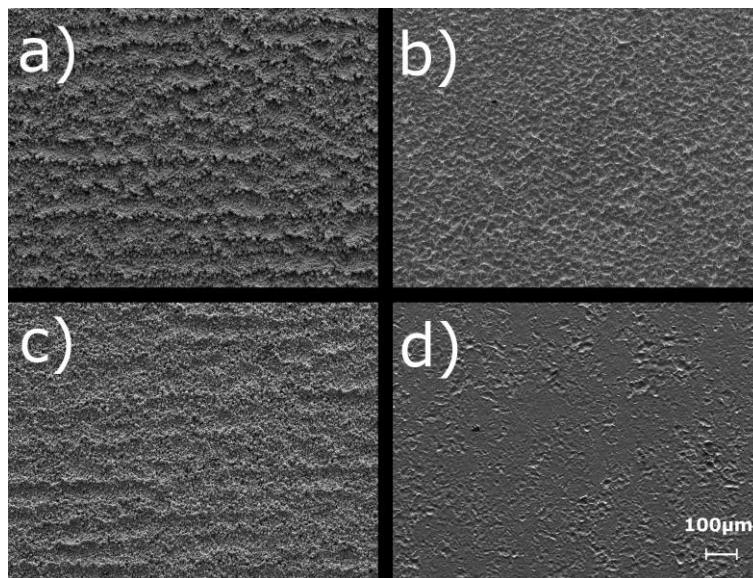


**Fig. 2** SEM images of modified samples surfaces at a magnification of 100 x: a) sample C; b) sample W1; c) sample O1; d) sample O3

Detailed morphology of the machined surfaces was observed at a magnification of 1500 x. Samples C and O1 (Fig. 3 a) c)) contain solidified globular structures up to 4 μm. The surface of sample W1 (Fig. 3 b)) and W3 was characterized by corrugation and a re-melted layer with a smooth surface. There were large numbers of microcracks on both surfaces. The surface of the O3 sample (Fig. 3 d)) was characterized by a small number of cracks and a rare smooth spatter of the material.

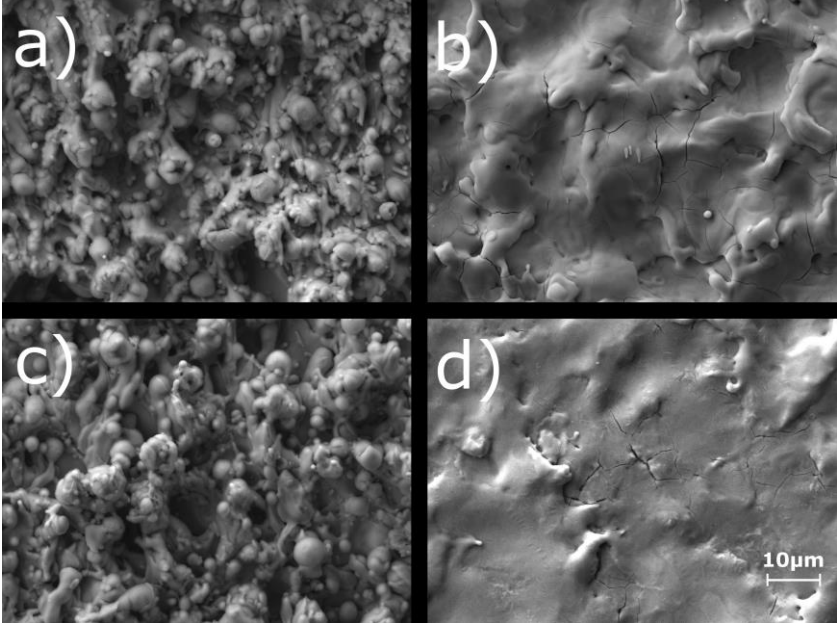


**Fig. 3** SEM images of modified samples surfaces at a magnification of 1500 x: a) sample C; b) sample W1; c) sample O1; d) sample O3

**Area Surface Roughness**

Surface roughness parameters were measured on a confocal microscope. Colour 3D topography maps of selected surfaces with profiles are shown in Fig. 4.

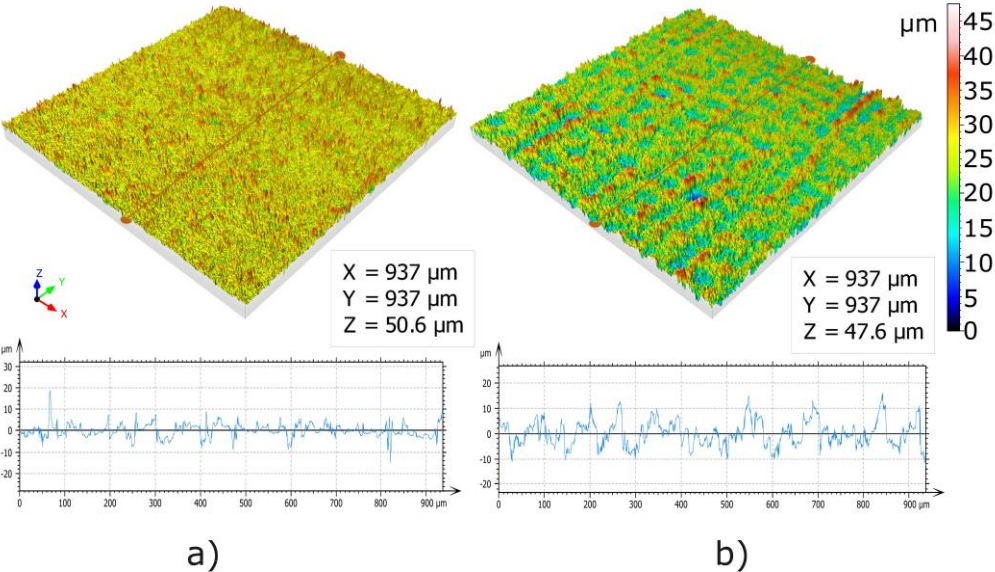


**Fig. 4** 3D colour maps of machined surfaces: a) sample W1; b) sample O1

The analysed surface roughness parameters are given in the Table 2. The surfaces of samples C and O1 showed similar surface roughness values, 4.97  $\mu\text{m}$  and 4.01  $\mu\text{m}$ , respectively. Samples W1 and W3 also showed very similar values, around  $\sim 2 \mu\text{m}$ . From these values, it is clear that LAL in water had an effect on the cooling and solidification mechanism of the material.

<b>Table 2</b> Measured area roughness parameters ( $\mu\text{m}$ )						
	<b>Sa</b>	<b>Sq</b>	<b>Sp</b>	<b>Sv</b>	<b>Ssk</b>	<b>Sku</b>
<b>Sample C</b>	4.97	6.25	29.7	22.1	0.27	3.12
<b>Sample W1</b>	2.08	2.85	22.2	28.3	-0.11	5.90
<b>Sample W3</b>	2.00	2.80	25.7	29.4	0.069	6.74
<b>Sample O1</b>	4.01	5.04	25.9	21.6	0.164	3.11
<b>Sample O3</b>	0.582	0.883	17.6	12.1	1.63	16.4

### Heat Affected Zone

The heat affected area was observed in the sections of the samples. Heat affected area of samples C in different scale is shown in Fig. 5. The thickness of affected area is more than 10  $\mu\text{m}$ . Sample C also show large values of surface roughness. Similar values of heat affected area were observed on O samples Fig 6 b). The smallest heat affected area can be observed in W samples Fig. 6 a). The width of the heat-treated layer in W samples is less than 5  $\mu\text{m}$ .

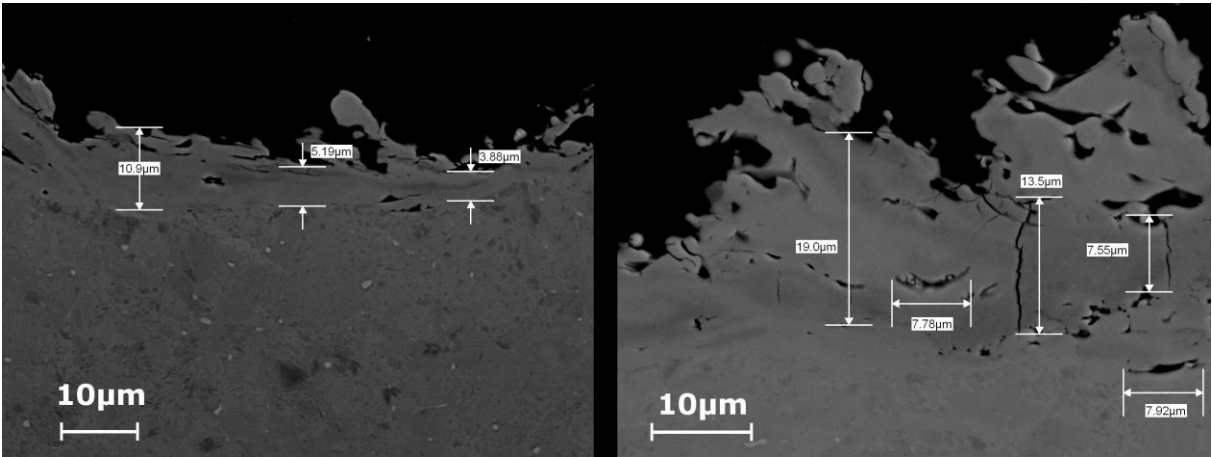


*Fig. 5 Heat affected area of sample C in different scale*

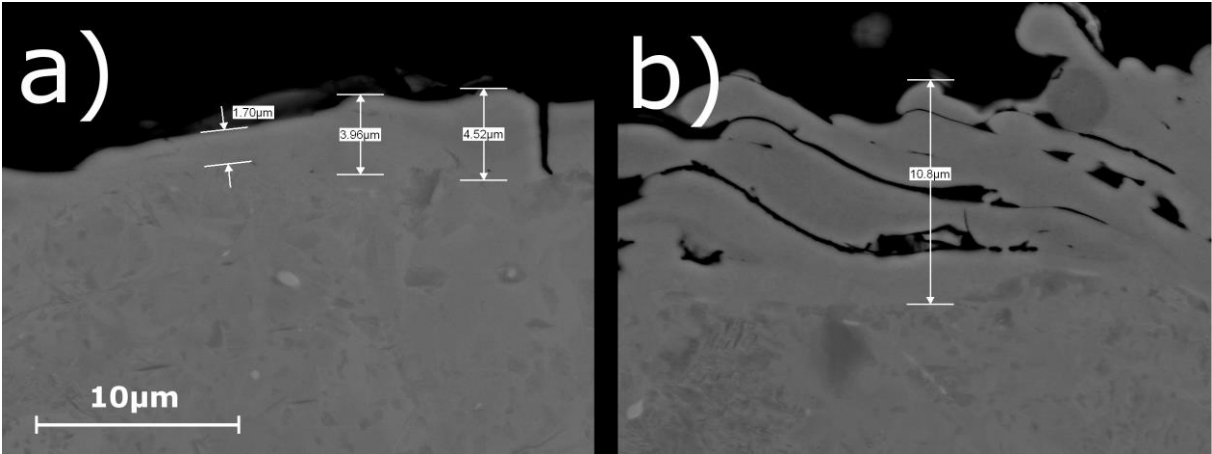


*Fig. 6 Heat affected area: a) sample W1; b) sample O1*

## Chemical Composition of the Surface

The elemental composition on the surfaces of processed samples was determined by WDS analysis. Measurements were made three times in different places on each surface. The measured values of weight % of individual elements are given in the Table 3. Due to the high reactivity of titanium with light elements from the environment at high temperatures, the aim was to determine the amount of diffuse elements into the machined surfaces.

	<b>Ti</b>	<b>O</b>	<b>N</b>	<b>C</b>
<b>Sample C</b>	66.74 ± 1.71	26.44 ± 1.84	4.41 ± 0.03	2.39 ± 0.16
<b>Sample W1</b>	74.88 ± 0.12	16.69 ± 0.16	6.95 ± 0.05	1.48 ± 0.01
<b>Sample W3</b>	76.02 ± 0.11	16.15 ± 0.16	7.17 ± 0.05	0.65 ± 0.005
<b>Sample O1</b>	66.13 ± 0.18	27.05 ± 0.19	4.01 ± 0.03	2.81 ± 0.02
<b>Sample O3</b>	77.49 ± 0.13	13.50 ± 0.34	5.39 ± 0.26	3.45 ± 0.11

## DISCUSSION

When the laser beam interacts with the surface of the titanium sample, the material is dynamically eroded by the movement of the laser beam along the scanned plane [8]. If the intensity of the radiation is high enough to overcome the melting threshold, these changes are reflected mainly in the surface morphology [16]. Two types of morphology were observed after LAL. The input parameters were constant for each sample, so it can be stated that the differences in morphology were caused by the presence and type of used fluid. The first two surfaces (samples C and O1) boil markedly rough with similar spherical solidified formations. Another characteristic type was formed on samples W 1 and W3, which were characterized by a smooth wavy surface with numerous cracks. The third one was the surface of sample O3, where the material removal was almost non-existing, irregularly spaced laser pulse tracks and cracks are present on the surface. The formation of these specific surfaces is caused by chemical and physical changes during machining, which are physical phenomena such as the transmission of light by liquid, liquid vaporization, bubble formation, growth and collapse, plasma formation, and expansion [17].

When a high-intensity laser beam ( $> 10 \text{ GW.cm}^{-2}$ ) interacts with a metal sample immersed in liquid, during surface melting, the atomization of workpiece particles and the decomposition of liquid occur [6]. Plasma of high density, high pressure (in the range of 10 GPa) and high temperature (4000 to 6000 K) is obtained due to the confinement effects of the liquid [18,19]. The initial dense plasma plume expanded, and as the energy was transferred to the surrounding liquid, the liquid molecules evaporated. The main difference between laser ablation in liquid and that in controlled gas atmosphere is that, as the plume expands adiabatically with supersonic velocity within the liquid in which the target is immersed, it experiences an additional confinement effect from the liquid. This expansion of matter through evaporation causes shock waves in the liquid, which spread at a rate of approximately  $1500 \text{ m.s}^{-1}$  in water [6].

The layer of steam produced around the laser-induced plasma can grow into a cavitation bubble that expands and then collapses on a time scale of several 100 microseconds. According to the research in [19], the consequent dense cloud of titanium species so generated leads to the formation of embryonic Ti clusters, which were observed on all machined surfaces. At the same time, laser-water interactions may cause photodissociation of

the water due to one- or multiple-photon excitation and the formation of bubbles at the laser spot. The vaporization of water at the plume – liquid interface and its breakdown into water vapor, atomic and molecular hydrogen or oxygen are called ‘water plasma’ [19].

The interactions between the water plasma and the active metal clusters provide the diffusion of carbon, the oxidation of metallic Ti, and the final formation of the  $Ti_xO_y$  nanostructure formed by chemical reactions [19]. During the recrystallization process at the solid-liquid interface, oxygen / hydrogen was diffused to the target surface [18]. According to [14], titanium incorporates oxygen from water during ablation, resulting in ~16.50 wt. % of  $O_2$ . In the case of samples C and O1, the amount of  $O_2$  reached 26.44 wt. % due to the large amount of remelted material. Titanium is known to react at higher temperatures, and in these cases the surface has been significantly remelted compared to the surface when it is machining in water, so that oxygen has diffused into a larger volume of material. It has been reported in [19] that the primary products of the laser ablation of titanium in water were hydroxides, which formed clusters of hydroxide nanoparticles or transform into oxide.

As a result of plasma shielding, many liquid waves and cracks are produced in the Ti alloy in research work in [5]. Due to the high energy density of the laser radiation, several cracks also occurred on the samples machined in the water, W1 and W3. According to the authors, the low thermal conductivity of titanium ( $8.08 \text{ W}\cdot\text{m}^{-1}\cdot\text{K}^{-1}$ ) caused crack formation. After laser irradiation, rapid heating and cooling of the titanium target are responsible for cracks [5]. Resolidified material accumulation was observed in the case of samples C and O1. The droplets are attributable to hydrodynamical sputtering. Kanitz et al. [20] explained the formation of droplets on the surface. High laser intensities may lead to an instability of the molten layer, which induces nanodroplet formation through thin layer disintegration and jetting from the molten surface [20].

Multiple arrangements of the formed craters can be caused by nonuniformities, inhomogeneities, voids, and chemical modification of the material, especially by the formation of oxides, hydrides, and carbides at the surface. These inconsistencies and chemical changes are responsible for nonuniform energy deposits and therefore the size and distance between the craters are not uniform [18].

## CONCLUSION

Laser ablation in various environments has a significant effect on the overall ablation process and the resulting condition of the material surface. As a standard, the process of ablation in the open air or protective or inert gases are used. The experiments showed that even different liquid media can streamline the ablation process and improve the quality of the resulting surface. In addition, working with a liquid medium in the ablation process is less demanding on machine adaptation and tools requirements. When using a liquid medium of water, it turns out that there is better heat dissipation, and flushing out gases and debris generated during ablation, which has a positive effect on the resulting surface of the laser-affected sample.

## Acknowledgement

This research was supported by the VEGA 2/0135/20 research project provided by the Ministry of Education, Science, Research and Sport of the Slovak Republic.

## References

- [1] SAHU, A.K., MALHOTRA, J., JHA, S. 2022. Laser-based hybrid micromachining processes: A review. *Opt. Laser Technol.* 146, 107554, doi:10.1016/J.OPTLASTEC.2021.107554.

- [2] YUHONG, L., LIANGCAI, X., TIELIN, S. 2011. The research on mechanical effect etching Si in pulsed laser micromachining under water. *Appl. Surf. Sci.*, 257, 3677–3681, doi:10.1016/j.apsusc.2010.11.105.
- [3] TANGWARODOMNUKUN, V., LIKHITANGSUWAT, P., TEVINPIBANPHAN, O., DUMKUM, C. 2015. Laser ablation of titanium alloy under a thin and flowing water layer. *Int. J. Mach. Tools Manuf.*, 89, 14–28, doi:10.1016/j.ijmachtools.2014.10.013.
- [4] ALI, N., BASHIR, S., UMM-I-KALSOOM; BEGUM, N., RAFIQUE, M.S., HUSINSKY, W. 2017. Effect of liquid environment on the titanium surface modification by laser ablation. *Appl. Surf. Sci.*, 405, 298–307, doi:10.1016/J.APSUSC.2017.02.047.
- [5] OUYANG, P., LI, P., LEKSINA, E.G., MICHURIN, S. V., HE, L. 2016. Effect of liquid properties on laser ablation of aluminum and titanium alloys. *Appl. Surf. Sci.*, 360, 880–888, doi:10.1016/J.APSUSC.2015.11.080.
- [6] FORSYTHE, R.C., COX, C.P., WILSEY, M.K., MÜLLER, A.M. 2021. Pulsed Laser in Liquids Made Nanomaterials for Catalysis. *Chem. Rev.*, 121, 7568–7637, doi:10.1021/ACS.CHEMREV.0C01069.
- [7] LIANG, C., SHIMIZU, Y., SASAKI, T., KOSHIZAKI, N. 2004. Synthesis, characterization, and phase stability of ultrafine TiO<sub>2</sub> nanoparticles by pulsed laser ablation in liquid media. *J. Mater. Res.* 2004 195, 19, 1551–1557, doi:10.1557/JMR.2004.0208.
- [8] KOCHUEV, D.A., KHORKOV, K.S., ABRAMOV, D. V., ARAKELIAN, S.M., PROKOSHEV, V.G. 2018. Titanium-Carbide Formation in a Liquid Hydrocarbon Medium by Femtosecond Laser Irradiation. *J. Surf. Investig.* 12, 1220–1223, doi:10.1134/S1027451018050622/FIGURES/3.
- [9] BASHIR, S., RAFIQUE, M.S., NATHALA, C.S., HUSINSKY, W. 2014. Surface and structural modifications of titanium induced by various pulse energies of a femtosecond laser in liquid and dry environment. *Appl. Phys. A Mater. Sci. Process.*, 114, 243–251, doi:10.1007/S00339-013-8116-2/FIGURES/6.
- [10] SEMALTIANOS, N.G., LOGOTHETIDIS, S., FRANGIS, N., TSIAOUSSIS, I., PERRIE, W., DEARDEN, G., WATKINS, K.G. 2010. Laser ablation in water: A route to synthesize nanoparticles of titanium monoxide. *Chem. Phys. Lett.* 496, 113–116, doi:10.1016/J.CPLETT.2010.07.023.
- [11] SERKOV, A.A., BARMINA, E. V., SHAFEEV, G.A., VORONOV, V. V. 2015. Laser ablation of titanium in liquid in external electric field. *Appl. Surf. Sci.*, 348, 16–21, doi:10.1016/J.APSUSC.2014.12.139.
- [12] ALBU, C., DINESCU, A., FILIPESCU, M., ULMEANU, M., ZAMFIRESCU, M. 2013. Periodical structures induced by femtosecond laser on metals in air and liquid environments. *Appl Surf Sci*, 278, 347, doi:10.1016/j.apsusc.2012.11.075.
- [13] CHATURVEDI, A., JOSHI, M.P., MONDAL, P., SINHA, A.K., SRIVASTAVA, A.K. 2017. Growth of anatase and rutile phase TiO<sub>2</sub> nanoparticles using pulsed laser ablation in liquid: Influence of surfactant addition and ablation time variation. *Appl. Surf. Sci.*, 396, 303–309, doi:10.1016/J.APSUSC.2016.10.133.
- [14] GOLIGHTLY, J.S., CASTLEMAN, A.W. 2006. Analysis of Titanium Nanoparticles Created by Laser Irradiation under Liquid Environments†. *J. Phys. Chem. B*, 110, 19979–19984, doi:10.1021/JP062123X.
- [15] KRSTULOVIĆ, N., SHANNON, S., STEFANUIK, R., FANARA, C. 2013. Underwater-laser drilling of aluminum. *Int. J. Adv. Manuf. Technol.*, 69, 1765–1773, doi:10.1007/S00170-013-5141-4.
- [16] ABRAMOV, D. V., ARAKELYAN, S.M., MAKOV, S.A., PROKOSHEV, V.G., KHOR'KOV, K.S. 2013. Formation of a system of microcraters on a titanium surface by femtosecond laser radiation under rapid cooling conditions. *Tech. Phys. Lett.*, 39, 719, doi:10.1134/s1063785013080154.
- [17] BEHERA, R.R., SANKAR, M.R., SWAMINATHAN, J., KUMAR, I., SHARMA, A.K., KHARE, A. 2016. Experimental investigation of underwater laser beam micromachining (UW-LB $\mu$ M) on 304 stainless steel. *Int. J. Adv. Manuf. Technol.*, 85, 1969–1982, doi:10.1007/S00170-016-8635-Z.
- [18] ALI, N., BASHIR, S., UMM-I-KALSOOM, AKRAM, M., MAHMOOD, K. 2013. Effect of dry and wet ambient environment on the pulsed laser ablation of titanium. *Appl Surf Sci*, 270, 49, doi:10.1016/j.apsusc.2012.12.049.
- [19] DE BONIS, A., GALASSO, A., IBRIS, N., LAURITA, A., SANTAGATA, A., TEGHIL, R. 2013. Rutile microtubes assembly from nanostructures obtained by ultra-short laser ablation of titanium in liquid. *Appl. Surf. Sci.*, 268, 571–578, doi:10.1016/J.APSUSC.2013.01.015.

- [20] KANITZ, A., KALUS, M.R., GUREVICH, E.L., OSTENDORF, A., BARCIKOWSKI, S., AMANS, D. 2019. Review on experimental and theoretical investigations of the early stage, femtoseconds to microseconds processes during laser ablation in liquid-phase for the synthesis of colloidal nanoparticles. *Plasma Sources Sci. Technol. Plasma Sources Sci. Technol*, 28, 34, doi:10.1088/1361-6595/ab3dbe.

## ORCID

Barbora Bočáková	0000-0002-4549-3908
Martin Necpal	0000-0003-2142-9204
Martin Sahul	0000-0001-9472-500X